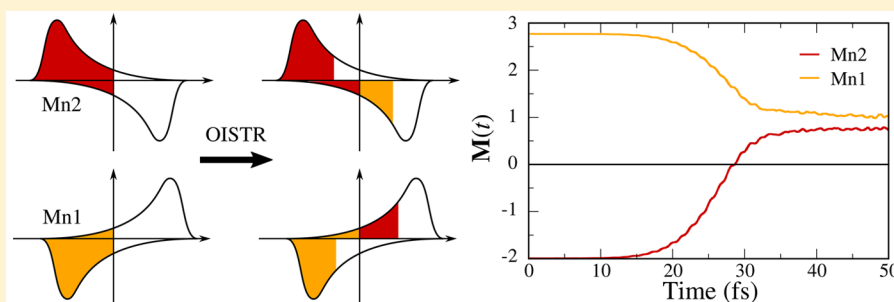


## Laser-Induced Intersite Spin Transfer

John Kay Dewhurst,<sup>†</sup> Peter Elliott,<sup>†</sup> Sam Shallcross,<sup>‡</sup> Eberhard K. U. Gross,<sup>†</sup> and Sangeeta Sharma<sup>\*,†</sup>

<sup>†</sup>Max-Planck Institut für Mikrostrukture Physics, Weinberg 2, D-06120 Halle, Germany

<sup>‡</sup>Lehrstuhl für Theoretische Festkörperphysik, Staudstrasse 7-B2, 91058 Erlangen, Germany



**ABSTRACT:** Laser pulses induce spin-selective charge flow that we show to generate dramatic changes in the magnetic structure of materials, including a switching of magnetic order from antiferromagnetic (AFM) to transient ferromagnetic (FM) in multisub-lattice systems. The microscopic mechanism underpinning this ultrafast switching of magnetic order is dominated by spin-selective charge transfer from one magnetic sublattice to another. Because this spin modulation is purely optical in nature (i.e., not mediated indirectly via the spin–orbit interaction) this is one of the fastest means of manipulating spin by light. We further demonstrate this mechanism to be universally applicable to AFM, FM, and ferri-magnets in both multilayer and bulk geometry and provide three rules that encapsulate early-time magnetization dynamics of multisub-lattice systems.

**KEYWORDS:** *Ultrafast spin manipulation, optical switching, multilayers, ab initio theory*

The type of magnetic coupling between the constituent atoms of a solid, i.e., ferromagnetic, antiferromagnetic, or noncollinear, is one of the most fundamental properties of any magnetic material. This magnetic order is governed by the exchange interaction, which is associated (from the energy–time uncertainty relation) with a characteristic time scale at which spin-flip scattering processes occur and change the intrinsic magnetic structure.<sup>1,2</sup> These time scales can be determined from the exchange parameters and are of the order of 40–400 fs for transition metal systems.<sup>3</sup> (The energy–time uncertainty relation provides a lower bound on the time scale associated with a spin flip:  $\hbar/J$ , with  $J$  being the energy cost of the spin flip, which is twice the exchange interaction in the Heisenberg model. This provides a rule-of-thumb for the time scale on which the exchange interaction can alter the intrinsic magnetic order of a material via spin flip scattering processes.) By employing laser pulses, researchers are currently attempting to manipulate the magnetic structure of materials at ultrashort time scales (sometimes even faster than exchange times). This manipulation ranges from spin-injection<sup>4–8</sup> and spin-transfer torque<sup>9–12</sup> across tailored interfaces to all-optical switching and ultrafast demagnetization. These efforts<sup>13–26</sup> point to rich underlying mechanisms that could contribute toward subexchange spin control.<sup>27–32</sup>

In this work, we demonstrate that spin transfer driven by intersite spin-selective charge transfer is one of the key mechanisms that underpins spin manipulation at sub-exchange time scales. This charge flow is induced by optical excitations

and represents both the fastest possible response of an electronic system to a laser pulse and as one highly sensitive to pulse intensity and structure. By investigating a wide range of interfaces and multisub-lattice magnetic materials, we demonstrate a rich phenomena of subexchange spin manipulation, including even changing the magnetic order of a material from AFM to FM on femtosecond time scales.<sup>2,33–44</sup> We furthermore are able to formulate three simple rules that predict the early time qualitative magnetization dynamics for ferromagnetic, antiferromagnetic and ferri-magnetic materials.

To study the early time charge and spin dynamics, we employ laser pulses of full width at half-maximum (fwhm) of about 20 fs. To be predictive, all simulations are performed in a fully ab initio manner employing a two-step process. In the first step we employ density functional theory (DFT) to obtain the ground-state magnetic order. In the second step the dynamics of the magnetization density under the influence of a laser pulse is simulated using the time-dependent extension of density functional theory (TD-DFT). These simulations are performed using a fully noncollinear version of TD-DFT, where the dynamics of charge and spins are treated beyond the linear response regime (for further technical details see methods and computational details).

**Received:** December 5, 2017

**Revised:** February 8, 2018

**Published:** February 9, 2018

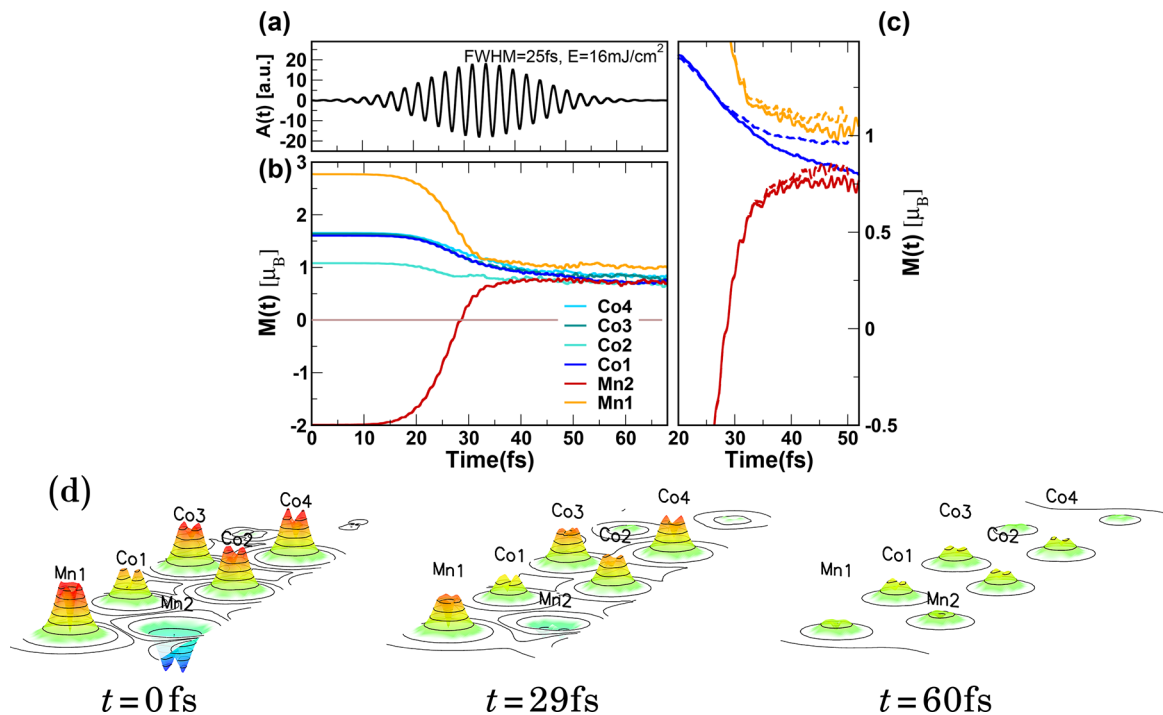


**Figure 1.** Laser-induced ultrafast change of magnetic order. (a) The pump laser pulse. (b) Time evolution of the layer resolved local magnetic moment in a Co/Mn multilayer, which at  $t = 0$  fs (i.e., in the ground state) is an antiferromagnet. At  $\sim 29$  fs, the interface Mn layer (that is coupled antiferromagnetically to all other layers at  $t = 0$ ) demagnetizes and then remagnetizes but with the spin orientation reversed. The magnetic order thus switches from uncompensated antiferromagnetic to transient ferromagnetic. (c) Time evolution of the layer resolved local magnetic moment with (full lines) and without (dashed lines) the spin-orbit coupling term, evidently switching of the magnetic order occurs before spin-orbit coupling has any significant impact on the dynamics. (d) Snapshots of the magnetization density density at  $t = 0, 29,$  and  $60$  fs.

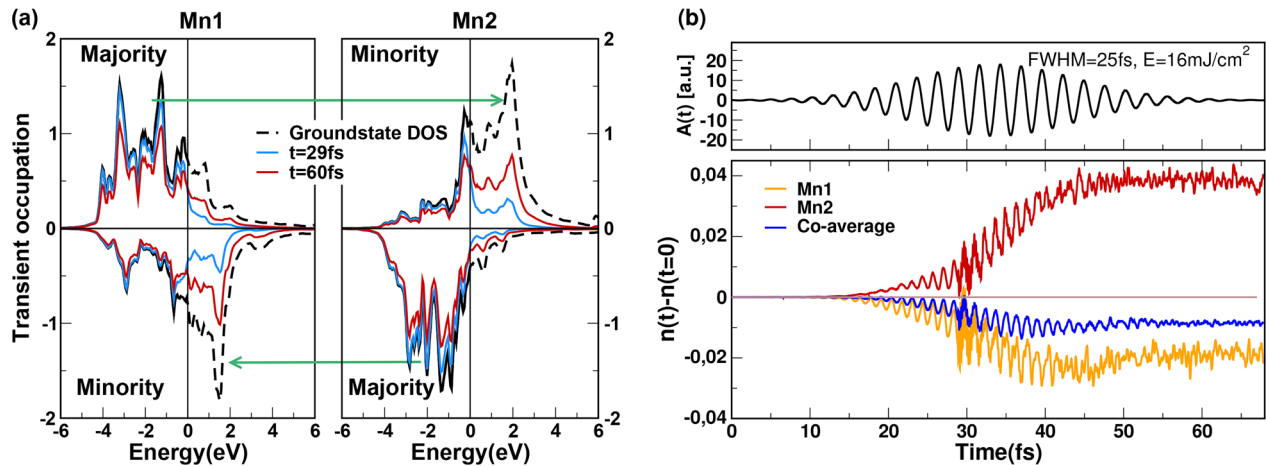


**Figure 2.** Microscopic origin of the transient all-optical switching of spin order observed in this work. (a) The time-dependent occupation of Kohn-Sham states for the two Mn layers (referred to as Mn1 and Mn2) whose spin dynamics are shown in Figure 1. At  $t = 0$ , these occupation numbers are equal to the ground-state density of states. Occupied states are shown with solid lines and empty with dashed line. The transient Kohn-Sham occupation numbers are presented for two different times: at  $t = 29$  fs (red line), at which the Mn2 totally demagnetizes before flipping its direction of moment, and at  $t = 60$  fs (blue line), where the spin order fully changes from AFM to FM. The change in magnetic order is driven by spin-selective charge flow of majority Mn1 states to minority Mn2 states and majority Mn2 states to minority Mn1 states (this flow of spin-selective charge is indicated by green arrows). (b) Dynamics of the spin-integrated charge ( $n_{\text{majority}} + n_{\text{minority}}$ ) in Mn1 and Mn2 and averaged over the four Co layers. These results indicate that while the spin-selective flow of charge dramatically changes magnetic structure, there is almost no significant change in the total charge on any of the constituent atoms of the multilayer in the first 29 fs.

**Multilayers.** We first consider a multilayer system consisting of two monolayers (ML) of Mn and four ML of Co, on a Cu(001) substrate. In the ground state, this system has a magnetic configuration in which the Mn layer at the Co interface is AFM-coupled to all other layers, with all moments oriented in-plane. The ground-state magnetic moment of each

layer can be seen in Figure 1b, along with the time evolution of these moments under the influence of a linearly polarized (in plane polarization) laser pulse with full width at half-maximum (fwhm) of 25 fs and fluence of 16 mJ/cm<sup>2</sup>. The spin dynamics are dramatically different for the different constituents of the multilayer: while the Co layers show very little change in spin

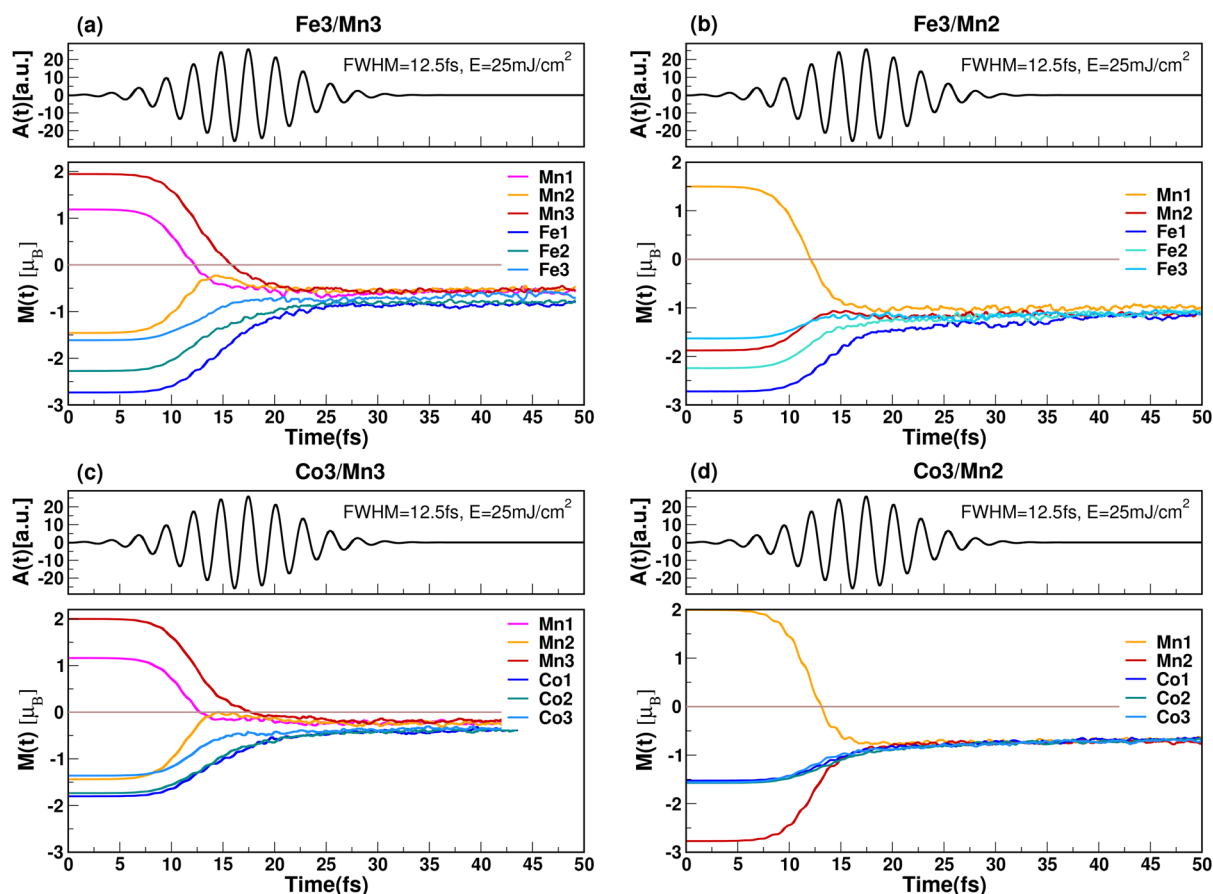


**Figure 3.** Switching of magnetic order in Fe/Mn and Co/Mn multilayers. The universality of the optically induced spin transfer (OISTR) mechanism can be seen in the time evolution of the local moment structure of different multilayers: (a) Fe with 3 Mn layers, (b) Fe with 2 Mn layers, (c) Co with 3 Mn layers, and (d) Co with 2 Mn layers. In all cases, the ultrashort laser pulse induces a change in magnetic order between 12 and 15 fs. The fwhm (12.5 fs) of the pulse and the time scale of the switching of magnetic order (12–15 fs) can be contrasted with Figure 1, in which a pulse of fwhm of 25 fs produced switching at 30 fs, a correlation of pulse fwhm and spin-switching time that follows from the purely optical excitations that underpin OISTR.

polarization, the two Mn layers demagnetize strongly under the influence of the laser pulse. Most interestingly, at  $\sim 29$  fs (slightly before peak intensity of the laser pulse) the interface AFM-coupled Mn layer switches the direction of its moment, thus changing the magnetic order of the multilayer from AFM to FM. Beyond this point, the layers remain in this transient FM state for a long time (at least up to 150 fs, at which point our simulation ended). Between 40 and 150 fs, all layers gradually demagnetize. The physics of this demagnetization were found to be dominated by spin-orbit induced spin-flips, similar to that which we observed previously for elemental magnets.<sup>45–47</sup> In the absence of spin-orbit coupling, the total spin moment is a good quantum number (i.e., stays constant with time); however, local moments may change. The impact of spin-orbit coupling on the early time dynamics of these local-moments is shown in Figure 1c, from which it is clear that below 40 fs the effect of spin-orbit coupling is insignificant. The dynamics of the full magnetization vector field can be seen in Figure 1d, where we show the layer projected magnetization as a function of time. A switching of the spin direction of Mn2 at  $t = 29$  fs can also be seen in this plot. These so-called 4D snapshots can be accessed via imaging experiments if soft X-rays are used as probes.

A closer inspection shows that the microscopic physics behind this dramatic change of the magnetic order is the

intersite flow of spin-selective charge, which may significantly alter magnetic moments while resulting in no significant change in the total charge on any of the constituent atoms of the multilayer. To demonstrate this in Figure 2, we show the transient occupation numbers<sup>48</sup> of the Kohn–Sham orbitals (see eq 2 in the Methods and Computational Details section) for the two Mn layers (at  $t = 0$ , these occupations numbers are the ground-state density of states). Because the Mn layers are AFM-coupled, the majority spin is oppositely oriented in each of these two layers: spin up is majority in the top layer (labeled Mn1), and spin-down is the majority in the interface layer (labeled Mn2). This electronic structure then allows purely optical excitations to drive spin up charge from the occupied majority Mn1 and Co (below the ground-state chemical potential) to the unoccupied minority Mn2 (above the chemical potential). Similarly, spin-down charge excitation occurs from majority Mn2 to minority Mn1. This spin selective flow of charge from one Mn layer to the another is indicated by the arrows in Figure 2. The optically induced charge flow from majority to minority spin channels then naturally leads to a loss of local moment in each layer with, at  $\sim 29$  fs, the interface layer (Mn2) becoming fully demagnetized. Continuation of this process then ultimately leads to a remagnetization of this layer, as there has been majority-minority inversion but with the spin orientation switched. In agreement with our previous finding

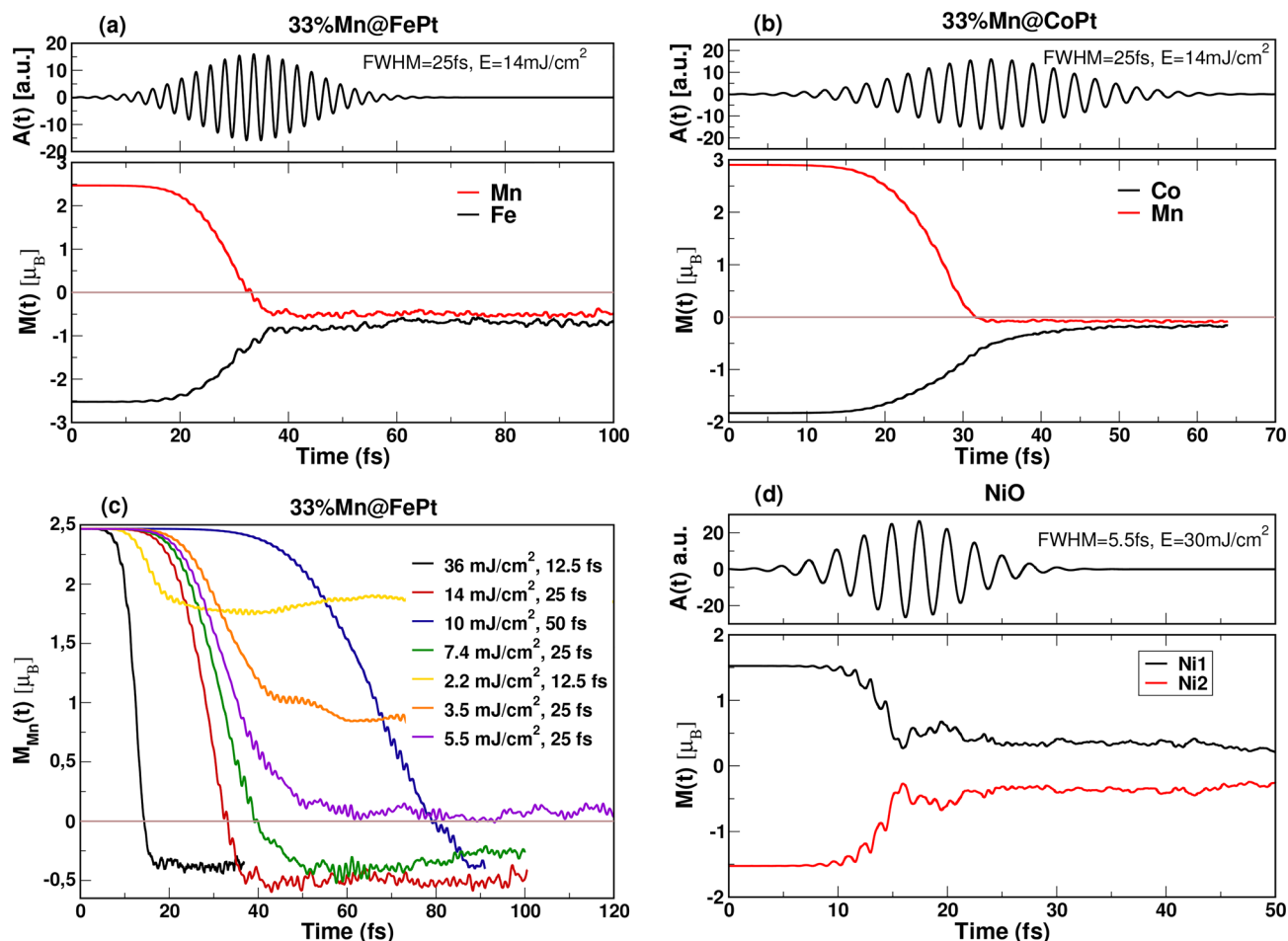


**Figure 4.** Ultrafast switching of magnetic order in bulk materials. The OISTR effect drives a switching of magnetic order also in bulk systems; shown are the dynamics of the local magnetic moments under the influence of laser pulse (shown in the top panels) for (a)  $L1_0$ -FePt with 33% Mn and (b)  $L1_0$ -CoPt with 33% Mn. In both cases, OISTR leads to switching of the magnetic order from AFM to transient FM. (c) Dynamics of magnetic moment on Mn sublattices in bulk Mn@FePt under the influence of seven different laser pulses given by the fluence ( $\text{mJ}/\text{cm}^2$ ) and fwhm (fs). (d) Dynamics of magnetization in NiO, which has two AFM-coupled lattices with the global moment zero. For such a perfectly compensated antiferromagnet, optically induced charge transfer can only lead to symmetric demagnetization.

(see Figure 1c) that spin orbit does not play a significant role, we find that during the first  $\sim 29$  fs, in which the local moments in the layers show strong dynamics, that the total moment of the system ( $M_{\text{Cu}} + M_{\text{Co}} + M_{\text{Mn}}$ ) remains almost unchanged ( $[M_{t=29} - M_{t=0}] / M_{t=0} < 0.02$ ). Purely optical excitations have thus bought about a change in the local moment structure leading to a switching of the global magnetic order, an effect we denote as an optically induced intersite spin transfer (OISTR). The time scale of OISTR is dictated by the amount of optically excited charge, which in turn is decided by the fluence and duration of the laser pulse, which, in the present case, is chosen to be significantly shorter than the exchange time of  $\sim 100$  fs.

Because the OISTR effect evidently involves significant flow of charge from the Mn1 majority to Mn2 minority and the Mn2 majority to Mn1 minority, there remains the possibility of a significant change in the total charge on Mn atoms resulting in development of a dipole moments. Having investigated the OISTR dynamics of the moment, we now therefore consider the dynamics of the local charge. As may be seen from Figure 2b, in which the spin-integrated charge ( $n_{\text{majority}} + n_{\text{minority}}$ ) is plotted for the Mn1 and Mn2 layers and averaged over the four Co layers, there is almost no change in the total charge on any constituent atoms of the multilayer. The optically induced spin

selective charge flow thus compensates: an approximately equal amount of minority electrons flow into the Mn layers as the majority electrons flow out of them. This indicates that this effect is best probed by spin-sensitive experiments, and distinguishes it from mechanisms in which spin and net charge flow coexist (such as the superdiffusive mechanism).<sup>49</sup>

Because the mechanism of OISTR relies on purely optical excitation of charge between the two sub-lattices, it might be expected that shorter and more intense laser pulses will produce correspondingly faster changes in magnetization. To validate this supposition, we now examine Fe/Mn and Co/Mn multilayers under the influence of shorter (fwhm of 12.5 fs) laser pulse than used in the previous case of Co/Mn multilayers (fwhm of 25 fs). The results for two and three Mn layers on Fe are shown in Figure 3a,b and for two and three Mn layers on Co in Figure 3c,d. The optical switching of magnetic order occurs in all four multilayers with, once again, the key feature responsible being OISTR, i.e., the spin-selective exchange of charge between majority and minority bands of AFM-coupled layers. Most importantly, in this case we see that switching of the magnetic order occurs at earlier times, between 12 and 15 fs, as opposed to the switching time of  $\sim 25$  fs for the Co/Mn

multilayer in Figure 1, perfectly consistent with the optical excitations that underpin OISTR.

**Bulk Materials.** We now demonstrate that OISTR also dominates early-time spin dynamics in bulk materials. To investigate this, we consider  $L1_0$  FePt with 33% Mn and  $L1_0$  CoPt with 33% Mn with, in each case, the Mn sub-lattice substituted to replace a Pt sublattice. The results for both of these systems are presented in Figure 4. In both cases, the Mn sub-lattices couple AFM to the other magnetic species (Fe/Co) in the ground state (with spins pointing in the  $c$ -direction). However, after application of the laser pulse, at  $\sim 30$  fs the magnetic order changes from AFM to transient FM. In both of these cases, the physics of the switching of magnetic order is OISTR, exactly the same mechanism as found in the case of multilayers.

The case of Mn@FePt, in which both sub-lattices have roughly the same moment ( $\sim 2.5 \mu_B$ ), is distinct from the case of Mn@CoPt, where Mn atoms have a large moment in the ground state ( $2.9 \mu_B$ ), while Co atoms have much smaller moments ( $1.9 \mu_B$ ). Due to this disparity in the local moments in Mn@CoPt, a larger amount of spin-selective charge transfer from Co to Mn (and vice versa) is required to switch the direction of magnetization. This is the reason for small moment on both Co and Mn sublattices after 30 fs, with the same laser pulse as used for the case of Mn@FePt.

In Figure 4c are plotted the dynamics of the moments of Mn atoms in bulk Mn@FePt under the influence of laser pulses of various fwhm and fluence. It is clear from these results that mechanism of OISTR is highly sensitive to pulse characteristics. First, as was seen in the case of the Co/Mn multilayers, the time scale of the switching from AFM to FM is strongly influenced by the fwhm of the laser pulse. Second, and most interestingly, it can be seen that final moment on the Mn atoms is almost the same for the four pulses, irrespective of the time scale on which the switching of magnetic order occurs. This follows from the fact that the final value of the moment is determined by the spin-selective exchange of charge from one sublattice to another, which is almost the same in all cases. This points toward the existence of a threshold fluence below which switching will not occur due to an insufficient number of excited electrons. Such results are also shown in Figure 4c for the case of short and low-intensity pulses, in which Mn demagnetizes due to OISTR but does not switch its direction of magnetization. These results demonstrate that the number of excited electrons is key to controlling early time spin-dynamics.

Finally, we address the question of how this physics manifests in FM systems and in fully symmetric AFM systems. In FM systems, for which the spin type of the majority channel is globally and not locally defined, such a spin-selective charge flows lead not to a change in magnetic order but simply to changes in the magnitude of local moments. A special case of this can be found in the Heusler alloys<sup>48</sup> for which a laser-induced dynamics causes an increase in the local moment on one sublattice, and a corresponding decrease on the other. For the case of perfect AFM, the OISTR mechanism can only lead to a symmetric demagnetization: the charge flow between majority and minority will be identical in both spin channels and can therefore only result in equal demagnetization of both sublattices.<sup>32</sup> To demonstrate this in Figure 4d, we show the spin dynamics of the antiferromagnet NiO; as can be seen, in place of the FM transient found for uncompensated AFM systems, the system simply symmetrically demagnetizes.

In conclusion, taken together, these results demonstrate the central importance of the local  $d$  (or  $f$ ) density of states in determining the optically induced charge transfer between the majority and minority channels. Our finding can be encapsulated in three simple rules that govern ultrashort time laser-induced spin-dynamics: (i) uncompensated antiferromagnets will, with sufficient fluence, change magnetic order from AFM to FM; (ii) fully compensated AFM materials will symmetrically demagnetize; and (iii) FM materials will show a change in the magnitude of their local moments but no change in magnetic order. The first of these rules underpins the optically induced ultrafast change in magnetic order observed in the present work. For high-fluence ultrashort laser pulses, this change in magnetic order can be achieved before spin-orbit coupling effects start to dominate or decohere the spin systems. Ultrashort-time-scale laser pulses that induce dynamics on time scales faster than exchange interaction thus encompass a rich variety of spin dynamics phenomena. Moreover, because the time scale of spin modulation is dictated by the fluence and duration of the laser pulse, and this mechanism offers a great deal of control over the spins via pulse design.

Experimentally, these predictions could be verified in a number of ways: (i) reduction of the full width half-maximum of the laser pulse should lead to the occurrence at earlier times of the ferromagnetic transient in spin-switching experiments; (ii) variation of pulse fluence should reveal the presence of a threshold fluence for the switching of magnetic order; (iii) as one of the sublattice fully demagnetizes and then remagnetizes again, the moment does not increase in the lateral directions; (iv) there are XMCD element-specific probes for the local moment dynamics; and (v) time-dependent spin and angle-resolved PES was performed after the application of the pump laser pulse.

**Method and Computational Details.** The Runge–Gross theorem<sup>50</sup> establishes that the time-dependent external potential is a unique functional of the time-dependent density, given the initial state. Based on this theorem, a system of noninteracting particles can be chosen such that the density of this non-interacting system is equal to that of the interacting system for all times.<sup>51–53</sup> The wave function of this non-interacting system is represented as a Slater determinant of single-particle orbitals. In what follows, a fully noncollinear spin-dependent version of these theorems is employed.<sup>45</sup> Next, the time-dependent Kohn–Sham (KS) orbitals are Pauli spinors determined by the equation:

$$i \frac{\partial \psi_j(\mathbf{r}, t)}{\partial t} = \left[ \frac{1}{2} \left( -i\nabla + \frac{1}{c} \mathbf{A}_{\text{ext}}(t) \right)^2 + v_s(\mathbf{r}, t) + \frac{1}{2c} \sigma \cdot \mathbf{B}_s(\mathbf{r}, t) + \frac{1}{4c^2} \sigma \cdot (\nabla v_s(\mathbf{r}, t) \times -i\nabla) \right] \psi_j(\mathbf{r}, t) \quad (1)$$

where  $\mathbf{A}_{\text{ext}}(t)$  is a vector potential representing the applied laser field, and  $\sigma$  are the Pauli matrices. The KS effective potential  $v_s(\mathbf{r}, t) = v_{\text{ext}}(\mathbf{r}, t) + v_{\text{H}}(\mathbf{r}, t) + v_{\text{xc}}(\mathbf{r}, t)$  is decomposed into the external potential  $v_{\text{ext}}$ , the classical electrostatic Hartree potential  $v_{\text{H}}$ , and the exchange-correlation (XC) potential  $v_{\text{xc}}$ . Similarly the KS magnetic field is written as  $\mathbf{B}_s(\mathbf{r}, t) = \mathbf{B}_{\text{ext}}(t) + \mathbf{B}_{\text{xc}}(\mathbf{r}, t)$ , where  $\mathbf{B}_{\text{ext}}(t)$  is the magnetic field of the applied laser pulse plus possibly an additional magnetic field and,  $\mathbf{B}_{\text{xc}}(\mathbf{r}, t)$  is the XC magnetic field. The final term of eq 1 is the spin-orbit coupling term. It is assumed that the wavelength of the applied laser is much greater than the size of a unit cell and the dipole

approximation can be used, i.e., the spatial dependence of the vector potential is disregarded. All of the implementations are done using the state-of-the-art full potential linearized augmented plane wave (LAPW) method. Within this method the core electrons (with eigenvalues 95 eV below Fermi energy) are treated fully relativistically by solving the radial Dirac equation, while higher-lying electrons are treated using the scalar relativistic Hamiltonian in the presence of the spin-orbit coupling. To obtain the two-component Pauli spinor states, the Hamiltonian containing only the scalar potential is diagonalized in the LAPW basis: this is the first variational step. The scalar states thus obtained are then used as a basis to set up a second-variational Hamiltonian with spinor degrees of freedom.<sup>54</sup> This is more efficient than simply using spinor LAPW functions; however, care must be taken to ensure that a sufficient number of first-variational eigenstates for the convergence of the second-variational problem are used.

We solve eq 1 for the electronic system alone. Coupling of the electronic system to the nuclear degrees of freedom is not included in the present work. Radiative effects, which can be included by simultaneously time-propagating Maxwell's equations, are also not included in the present work. At longer timescales, these effects are expected to contribute significantly.

Time- and energy-resolved occupation of Kohn–Sham states, shown in Figure 2, can be calculated using the following:

$$A(\omega, t) = \sum_{i=1}^{\infty} \int_{\text{BZ}} \delta(\omega - \varepsilon_{ik}) g_{ik}(t) \quad (2)$$

with

$$g_{ik}(t) = \sum_j n_{jk} |O_{ij}^k(t)|^2 \quad (3)$$

where  $n_{jk}$  is the occupation number of the  $j^{\text{th}}$  time-evolving orbital,  $\psi_j$ , and:

$$O_{ij}^k(t) = \int d^3r \phi_{ik}^*(\mathbf{r}) \psi_j(\mathbf{r}, t) \quad (4)$$

Here,  $\phi_i$  is the ground-state Kohn–Sham orbital. In the absence of any time-dependent perturbation  $\psi_{jk}(\mathbf{r}, t=0) = \phi_{jk}^*(\mathbf{r})$ , and eq 2 gives the ground-state density of states.

A fully noncollinear version of TDDFT as implemented within the Elk code<sup>55</sup> is used for all calculations. A regular mesh in  $\mathbf{k}$ -space of  $8 \times 8 \times 1$  for multilayers and  $8 \times 8 \times 8$  for bulk is used, and a time step of  $\Delta t = 0.1$  au is employed for the time-propagation algorithm.<sup>56</sup> A smearing width of 0.027 eV is used. Laser pulses used in the present work are linearly polarized (in plane polarization) with a frequency of 1.55 eV (red). For all ground-state calculations a full structural optimization was performed. For the case of Co4/Mn2 layers on Cu(001) substrate, the substrate was simulated by using 4 to 10 Cu ML. We found that for Cu layer thickness greater than 4 ML, the results do not change significantly. For the case of bulk FePt and CoPt systems the Pt atoms were substituted with Mn atoms to simulate Mn-doped FePt or CoPt. For 33% Pt substitution by Mn, a supercell (in  $c$ -direction) containing 3Fe, 2Pt and 1Mn atom was constructed. All calculations (except for NiO) were performed using adiabatic local spin density approximation (ALSDA). NiO, being a strongly correlated material, is not well-described by ALSDA, and hence, the ALSDA +  $U$ , with  $U = 5$  eV, was used. This value of  $U$  was kept constant during the time-propagation.

## AUTHOR INFORMATION

### Corresponding Author

\*E-mail: sharma@mpi-halle.mpg.de. Phone: +49-345-5582913.

### ORCID

Sangeeta Sharma: 0000-0001-8929-9376

### Author Contributions

S. Sharma framed the project. J. Dewhurst and S. Sharma wrote the major part of the Elk code. P. Elliott and S. Sharma performed all calculations. S. Shallcross and E. Gross helped with analysis. S. Sharma and S. Shallcross took the lead in writing the manuscript, to which all authors contributed.

### Notes

The authors declare no competing financial interest.

## ACKNOWLEDGMENTS

S. Sharma thanks QUTIF-SPP for funding. P. Elliott and S. Sharma acknowledge funding from DFG through grant no. SFB762.

## REFERENCES

- (1) Mathias, S.; La-O-Vorakiat, C.; Grychtol, P.; Granitzka, P.; Turgut, E.; Shaw, J. M.; Adam, R.; Nembach, H. T.; Siemens, M. E.; Eich, S.; Schneider, C. M.; Silva, T. J.; Aeschlimann, M.; Murnane, M. M.; Kapteyn, H. C. *Proc. Natl. Acad. Sci. U. S. A.* **2012**, *109*, 4792–4797.
- (2) Radu, I.; Vahaplar, K.; Stamm, C.; Kachel, T.; Pontius, N.; Duerr, H. A.; Ostler, T. A.; Barker, J.; Evans, R. F. L.; Chantrell, R. W.; Tsukamoto, A.; Itoh, A.; Kirilyuk, A.; Rasing, T.; Kimel, A. V. *Nature* **2011**, *472*, 205–208.
- (3) Pajda, M.; Kudrnovský, J.; Turek, I.; Drchal, V.; Bruno, P. *Phys. Rev. B: Condens. Matter Mater. Phys.* **2001**, *64*, 174402.
- (4) Laman, N.; Bieler, M.; van Driel, H. J. *Appl. Phys.* **2005**, *98*, 103507.
- (5) Cinchetti, M.; Heimer, K.; Wuestenberg, J.-P.; Andreyev, O.; Bauer, M.; Lach, S.; Ziegler, C.; Gao, Y.; Aeschlimann, M. *Nat. Mater.* **2009**, *8*, 115–119.
- (6) Rudolf, D.; La-O-Vorakiat, C.; Battiato, M.; Adam, R.; Shaw, J. M.; Turgut, E.; Maldonado, P.; Mathias, S.; Grychtol, P.; Nembach, H. T.; et al. *Nat. Commun.* **2012**, *3*, 1037.
- (7) Melnikov, A.; Razdolski, I.; Wehling, T. O.; Papaioannou, E. T.; Roddatis, V.; Fumagalli, P.; Aktsipetrov, O.; Lichtenstein, A. I.; Bovensiepen, U. *Phys. Rev. Lett.* **2011**, *107*, 076601.
- (8) Hofherr, M.; Maldonado, P.; Schmitt, O.; Berritta, M.; Bierbrauer, U.; Sadashivaiah, S.; Schellekens, A. J.; Koopmans, B.; Steil, D.; Cinchetti, M.; et al. *Phys. Rev. B: Condens. Matter Mater. Phys.* **2017**, *96*, 100403.
- (9) Nemeš, P.; Rozkotova, E.; Tesarova, N.; Trojanek, F.; De Ranieri, E.; Olejnik, K.; Zemen, J.; Novak, V.; Cukr, M.; Maly, P.; Jungwirth, T. *Nat. Phys.* **2012**, *8*, 411–415.
- (10) Schellekens, A. J.; Kuiper, K. C.; de Wit, R. R. J. C.; Koopmans, B. *Nat. Commun.* **2014**, *5*, 4333.
- (11) Razdolski, I.; Alekhin, A.; Ilin, N.; Meyburg, J. P.; Roddatis, V.; Dising, D.; Bovensiepen, U.; Melnikov, A. *Nat. Commun.* **2017**, *8*, 15007.
- (12) Laliu, M. L. M.; Helgers, P. L. J.; Koopmans, B. *Phys. Rev. B: Condens. Matter Mater. Phys.* **2017**, *96*, 014417.
- (13) Beaufort, E.; Merle, J.; Daunois, A.; Bigot, J. *Phys. Rev. Lett.* **1996**, *76*, 4250–4253.
- (14) Scholl, A.; Baumgarten, L.; Jacquemin, R.; Eberhardt, W. *Phys. Rev. Lett.* **1997**, *79*, 5146–5149.
- (15) Hohlfeld, J.; Matthias, E.; Knorren, R.; Bennemann, K. *Phys. Rev. Lett.* **1997**, *78*, 4861–4864.
- (16) Aeschlimann, M.; Bauer, M.; Pawlik, S.; Weber, W.; Burgermeister, R.; Oberli, D.; Siegmann, H. *Phys. Rev. Lett.* **1997**, *79*, 5158–5161.

- (17) Kirilyuk, A.; Kimel, A. V.; Rasing, T. *Rev. Mod. Phys.* **2010**, *82*, 2731–2784.
- (18) Koopmans, B.; van Kampen, M.; Kohlhepp, J.; de Jonge, W. *Phys. Rev. Lett.* **2000**, *85*, 844–847.
- (19) Mueller, G. M.; Walowski, J.; Djordjevic, M.; Miao, G.-X.; Gupta, A.; Ramos, A. V.; Gehrke, K.; Moshnyaga, V.; Samwer, K.; Schmalhorst, J.; Thomas, A.; Huetten, A.; Reiss, G.; Moodera, J. S.; Muenzenberg, M. *Nat. Mater.* **2009**, *8*, 56–61.
- (20) Carley, R.; Doebrich, K.; Frietsch, B.; Gahl, C.; Teichmann, M.; Schwarzkopf, O.; Wernet, P.; Weinelt, M. *Phys. Rev. Lett.* **2012**, *109*, 057401.
- (21) Sultan, M.; Atxitia, U.; Melnikov, A.; Chubykalo-Fesenko, O.; Bovensiepen, U. *Phys. Rev. B: Condens. Matter Mater. Phys.* **2012**, *85*, 184407.
- (22) von Korff Schmising, C.; Pfau, B.; Schneider, M.; Guenther, C. M.; Giovannella, M.; Perron, J.; Vodungbo, B.; Mueller, L.; Capotondi, F.; Pedersoli, E.; Mahne, N.; Luening, J.; Eisebitt, S. *Phys. Rev. Lett.* **2014**, *112*, 217203.
- (23) Eschenlohr, A.; Sultan, M.; Melnikov, A.; Berggaard, N.; Wieczorek, J.; Kachel, T.; Stamm, C.; Bovensiepen, U. *Phys. Rev. B: Condens. Matter Mater. Phys.* **2014**, *89*, 214423.
- (24) Kampfrath, T.; Sell, A.; Klatt, G.; Pashkin, A.; Maehrlin, S.; Dekorsy, T.; Wolf, M.; Fiebig, M.; Leitenstorfer, A.; Huber, R. *Nat. Photonics* **2010**, *5*, 31–34.
- (25) Kimel, A.; Kirilyuk, A.; Tsvetkov, A.; Pisarev, R.; Rasing, T. *Nature* **2004**, *429*, 850–853.
- (26) Fiebig, M.; Duong, N. P.; Satoh, T.; Van Aken, B. B.; Miyano, K.; Tomioka, Y.; Tokura, Y. *J. Phys. D: Appl. Phys.* **2008**, *41*, 164005.
- (27) Tudosa, I.; Stamm, C.; Kashuba, A.; King, F.; Siegmann, H.; Stohr, J.; Ju, G.; Lu, B.; Weller, D. *Nature* **2004**, *428*, 831–833.
- (28) Pouloupoulos, P.; Bovensiepen, U.; Farle, M.; Baberschke, K. *Phys. Rev. B: Condens. Matter Mater. Phys.* **1998**, *57*, 14036–14039.
- (29) Koch, R. H.; Grinstein, G.; Keefe, G. A.; Lu, Y.; Trouilloud, P. L.; Gallagher, W. J.; Parkin, S. S. P. *Phys. Rev. Lett.* **2000**, *84*, 5419–5422.
- (30) Wollmann, L.; Chadov, S.; Kuebler, J.; Felser, C. *Phys. Rev. B: Condens. Matter Mater. Phys.* **2015**, *92*, 064417.
- (31) Schaefer, M.; Drewello, V.; Reiss, G.; Thomas, A.; Thiel, K.; Eilers, G.; Muenzenberg, M.; Schuhmann, H.; Seibt, M. *Appl. Phys. Lett.* **2009**, *95*, 232119.
- (32) Simoni, J.; Stamenova, M.; Sanvito, S. *Phys. Rev. B: Condens. Matter Mater. Phys.* **2017**, *96*, 054411.
- (33) Stanciu, C. D.; Hansteen, F.; Kimel, A. V.; Kirilyuk, A.; Tsukamoto, A.; Itoh, A.; Rasing, T. *Phys. Rev. Lett.* **2007**, *99*, 047601.
- (34) Kirilyuk, A.; Kimel, A. V.; Rasing, T. *Rep. Prog. Phys.* **2013**, *76*, 026501.
- (35) Hansteen, F.; Kimel, A.; Kirilyuk, A.; Rasing, T. *Phys. Rev. Lett.* **2005**, *95*, 047402.
- (36) Acremann, Y.; Strachan, J. P.; Chembrolu, V.; Andrews, S. D.; Tyliszczak, T.; Katine, J. A.; Carey, M. J.; Clemens, B. M.; Siegmann, H. C.; Stohr, J. *Phys. Rev. Lett.* **2006**, *96*, 217202.
- (37) Stanciu, C.; Kimel, A.; Hansteen, F.; Tsukamoto, A.; Itoh, A.; Kirilyuk, A.; Rasing, T. *Phys. Rev. B: Condens. Matter Mater. Phys.* **2006**, *73*, 220402.
- (38) Liu, H.; Bedau, D.; Backes, D.; Katine, J. A.; Langer, J.; Kent, A. D. *Appl. Phys. Lett.* **2010**, *97*, 242510.
- (39) Li, T.; Patz, A.; Mouchliadis, L.; Yan, J.; Lograsso, T. A.; Perakis, I. E.; Wang, J. *Nature* **2013**, *496*, 69–73.
- (40) Graves, C. E.; et al. *Nat. Mater.* **2013**, *12*, 293–298.
- (41) Mangin, S.; Gottwald, M.; Lambert, C.-H.; Steil, D.; Uhlir, V.; Pang, L.; Hehn, M.; Alebrand, S.; Cinchetti, M.; Malinowski, G.; Fainman, Y.; Aeschlimann, M.; Fullerton, E. E. *Nat. Mater.* **2014**, *13*, 286.
- (42) Shcherbakov, M. R.; Vabishchevich, P. P.; Shorokhov, A. S.; Chong, K. E.; Choi, D.; Staude, I.; Miroshnichenko, A. E.; Neshev, D. N.; Fedyanin, A. A.; Kivshar, Y. S. *Nano Lett.* **2015**, *15*, 6985–6990.
- (43) Barker, J.; Atxitia, U.; Ostler, T. A.; Hovorka, O.; Chubykalo-Fesenko, O.; Chantrell, R. W. *Sci. Rep.* **2013**, *3*, 3262.
- (44) Lefkidis, G.; Huebner, W. *Phys. Rev. B: Condens. Matter Mater. Phys.* **2007**, *76*, 014418.
- (45) Krieger, K.; Dewhurst, J. K.; Elliott, P.; Sharma, S.; Gross, E. K. U. *J. Chem. Theory Comput.* **2015**, *11*, 4870–4874.
- (46) Krieger, K.; Elliott, P.; Müller, T.; Singh, N.; Dewhurst, J. K.; Gross, E. K. U.; Sharma, S. *J. Phys.: Condens. Matter* **2017**, *29*, 224001.
- (47) Shokeen, V.; Sanchez Piaia, M.; Bigot, J.-Y.; Müller, T.; Elliott, P.; Dewhurst, J. K.; Sharma, S.; Gross, E. K. U. *Phys. Rev. Lett.* **2017**, *119*, 107203.
- (48) Elliott, P.; Mueller, T.; Dewhurst, J. K.; Sharma, S.; Gross, E. K. U. *Sci. Rep.* **2016**, *6*, 38911.
- (49) Battiato, M.; Carva, K.; Oppeneer, P. M. *Phys. Rev. Lett.* **2010**, *105*, 027203.
- (50) Runge, E.; Gross, E. *Phys. Rev. Lett.* **1984**, *52*, 997.
- (51) Elliott, P.; Furche, F.; Burke, K. In *Reviews in Computational Chemistry*; Lipkowitz, K., Cundari, T., Eds.; Wiley, Hoboken, NJ, 2009; Vol. 26; pp 91–165.
- (52) Ullrich, C. A. *Time-Dependent Density-Functional Theory Concepts and Applications*; Oxford University Press: Oxford, NY, 2011.
- (53) Sharma, S.; Dewhurst, J. K.; Gross, E. K. U. In *First Principles Approaches to Spectroscopic Properties of Complex Materials*; Di Valentin, C., Botti, S., Cococcioni, M., Eds.; Springer Berlin Heidelberg: Berlin, Heidelberg, 2014; pp 235–257.
- (54) Singh, D. J. *Planewaves Pseudopotentials and the LAPW Method*; Kluwer Academic Publishers, Boston, 1994.
- (55) Dewhurst, J. K.; Sharma, S.; et al. *Elk code*, [elk.sourceforge.net](http://elk.sourceforge.net) (accessed Jan 14, 2018).
- (56) Dewhurst, J. K.; Krieger, K.; Sharma, S.; Gross, E. K. U. *Comput. Phys. Commun.* **2016**, *209*, 92–95.